JACS
JOURNAL OF THE AMERICAN CHEMICAL SOCIETY
pubs.acs.org/JACS
Article

# Isolation of a Bimetallic Cobalt(III) Nitride and Examination of Its Hydrogen Atom Abstraction Chemistry and Reactivity toward $H_2$

Debabrata Sengupta, Christian Sandoval-Pauker, Emily Schueller, Angela M. Encerrado-Manriquez, Alejandro Metta-Magaña, Wen-Yee Lee, Ram Seshadri, Balazs Pinter,* and Skye Fortier*

Cite This: J. Am. Chem. Soc. 2020, 142, 8233−8242



**ABSTRACT:** Room temperature photolysis of the bis(azide)cobaltate(II) complex $[Na(THF)_x][(^{ket}guan)Co(N_3)_2]$ ($^{ket}guan$ = $[(tBu_2CN)C(NDipp)_2]^-$, Dipp = 2,6-diisopropylphenyl) (**3a**) in THF cleanly forms the binuclear cobalt nitride $Na(THF)_4\{[(^{ket}guan)Co(N_3)]_2(\mu\text{-}N)\}$ (**1**). Compound **1** represents the first example of an isolable, bimetallic cobalt nitride complex, and it has been fully characterized by spectroscopic, magnetic, and computational analyses. Density functional theory supports a $Co^{III}{=}N{=}Co^{III}$ canonical form with significant $\pi$-bonding between the cobalt centers and the nitride atom. Unlike other group 9 bridging nitride complexes, no radical character is detected at the bridging N atom of **1**. Indeed, **1** is unreactive toward weak C−H donors and even cocrystallizes with a molecule of cyclohexadiene (CHD) in its crystallographic unit cell to give **1**·CHD as a room temperature stable product. Notably, addition of pyridine to **1** or photolyzed solutions of $[(^{ket}guan)Co(N_3)(py)]_2$ (**4a**) leads to destabilization via activation of the nitride unit, resulting in the mixed-valent Co(II)/Co(III) bridged imido species $[(^{ket}guan)Co(py)][(^{ket}guan)Co](\mu\text{-}NH)(\mu\text{-}N_3)$ (**5**) formed from intermolecular hydrogen atom abstraction (HAA) of strong C−H bonds (BDE ∼ 100 kcal/mol). Kinetic rate analysis of the formation of **5** in the presence of $C_6H_{12}$ or $C_6D_{12}$ gives a KIE = 2.5 ± 0.1, supportive of a HAA formation pathway. The reactivity of our system was further probed by photolyzing benzene/pyridine solutions of **4a** under $H_2$ and $D_2$ atmospheres (150 psi), which leads to the exclusive formation of the bis(imido) complexes $[(^{ket}guan)Co(\mu\text{-}NH)]_2$ (**6**) and $[(^{ket}guan)Co(\mu\text{-}ND)]_2$ (**6-D**), respectively, as a result of dihydrogen activation. These results provide unique insights into the chemistry and electronic structure of late 3d metal nitrides while providing entryway into C−H activation pathways.

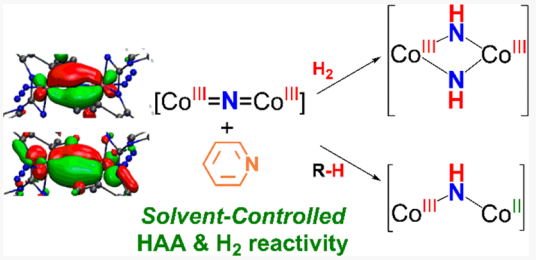


## INTRODUCTION

Complexes containing metal−ligand multiple bonds, both biological and synthetic, have been intensively investigated because of the participation of these moieties in a host of important reactions including C−H bond activation,[1] olefin metathesis,[2] cycloaddition,[3] and heteroatom transfer reactivity.[4] Indeed, the Fe=O intermediate formed in the active site of cytochrome P450 is critical for its enzymatic versatility.[5] Of note, isolable compounds containing M=E or M≡E bonds have been dominated by the early to mid-transition metals, while the synthesis and isolation of late metal complexes present a more significant challenge due to the progressive population of M=E/M≡E $\pi^*$-orbitals, leading to high reactivity and instability.[6−8]

In specific regard to group 9−11 metals in tetragonal ligand fields, it is considered the case that d-orbital occupation with electron counts of $n \geq 4$ is incompatible with metal−ligand multiple bonds, a concept that has been coined the "oxo wall".[5,9,10] Yet, the oxo wall can be circumvented through lowering the coordination number and symmetry, employing sterically encumbering ligands,[7,11,12] and reducing the d-electron count through metal oxidation.[6,8,13] These strategies have been effective for a handful of Rh/Ir compounds such as the iridium(V)oxo $Ir(O)(mes)_3$ (mes = mesityl) synthesized by Wilkinson[14] and nitride species such as (PNP)Ir(N) (PNP = $N(CHCHPtBu_2)_2$) reported by the groups of de Bruin and Schneider,[8] among others.[15−19] However, this can lead to nontrivial canonical forms, which complicates electronic structure interpretations and formal oxidation state assignments.[8,20]

Extension of these synthetic strategies to cobalt has afforded a number of imido complexes[13] and recently led to the isolation and structural characterization of the first terminal cobalt(III)−oxo species $[PhB(tBuIm)_3]Co(O)$ (Im = imidazol-2-ylidene).[21] Notably, though, terminal cobalt nitrides still remain elusive. In 2010, Chirik et al. reported that thermolysis or photolysis of ($^{iPr}$PDI)$CoN_3$ ($^{iPr}$PDI = 2,6-(2,6-$iPr_2$−$C_6H_3$−N=CMe)$_2C_5H_3N$) leads to intramolecular N-atom insertion, attributed to the formation of a fleeting terminal cobalt

Received: January 9, 2020
Published: April 11, 2020

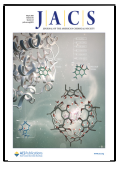

**Scheme 1. Synthetic Overview and HAA Reactivity with Alkanes and $H_2$**

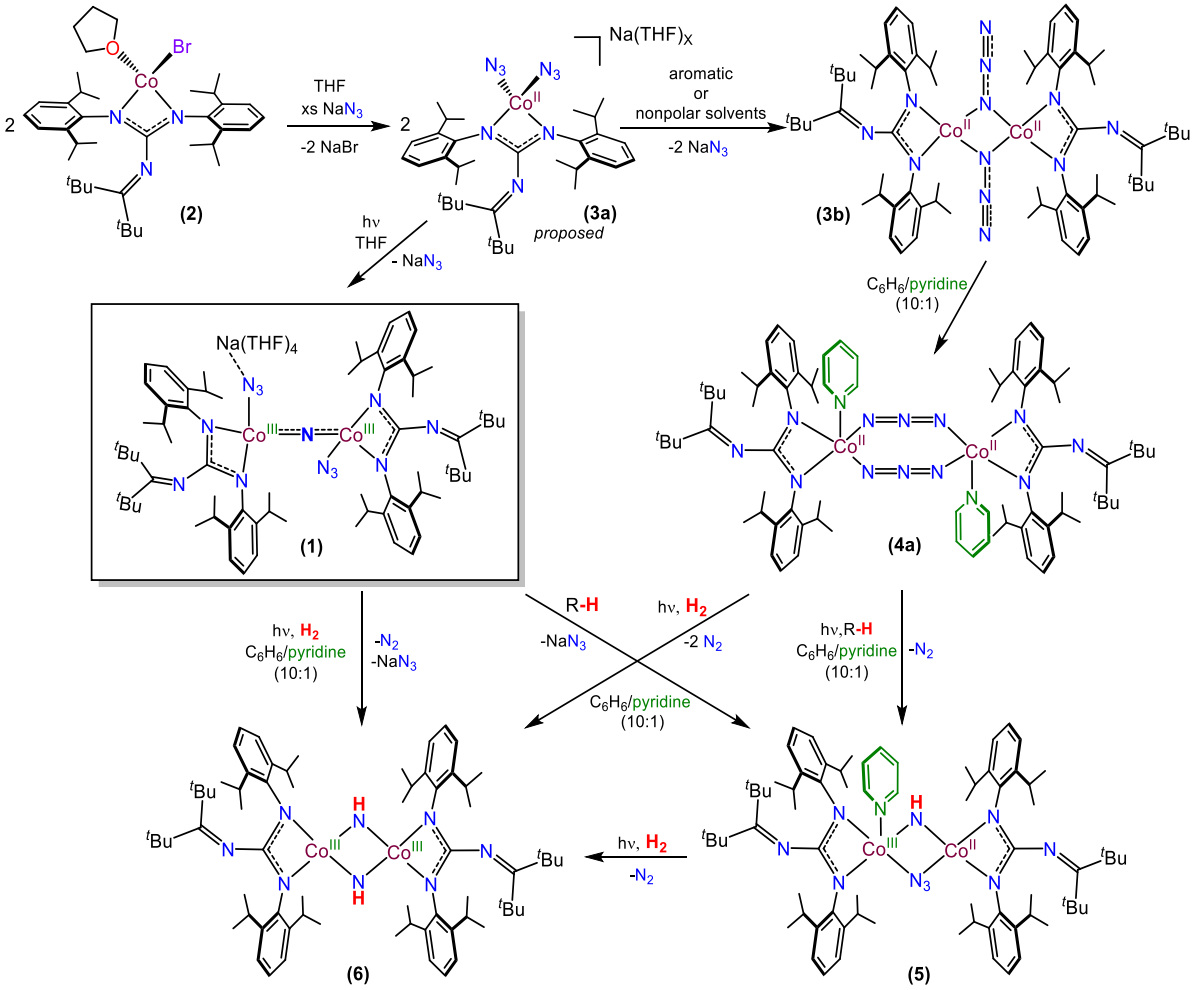


nitride.[22] Later, Meyer and co-workers were able to trap an intermediate nitride complex through the use of the bis(*N*-heterocyclic carbene)-mono(phenolate) chelated compound (BIMPN$^{Mes,Ad,Me}$)Co(N) at 10 K, which upon warming undergoes N-atom insertion into a Co−C bond.[23] Consequently, controlled reactivity studies of the cobalt−nitride moiety remain unknown.

It has come to light in recent years that the lifetime of Co═O complexes can be extended through the coordination of redox-inactive Lewis acids to the oxo moiety.[24,25] These compounds are still short-lived, but under this cooperative model, the second metal can alleviate charge density that would otherwise occupy antibonding orbitals, thereby extending lifetimes. Notably, Tomson and co-workers have capitalized upon this strategy utilizing macrocyclic pyridyl−diimine ligands to generate the putative dinuclear cobalt nitride $[(n\text{PDI}_2)\text{Co}_2(\mu\text{-N})(\text{PMe}_3)_2]^{3+}$.[26] This nitride is not observed, but its formation is indicated through the isolation of phosphinimide and intramolecular C−H amination products formed as the result of passing Co−N−Co formation. Building upon this approach of utilizing bimetallic systems to stabilize group 9 metal−ligand multiple bonds, we have targeted the synthesis of isolable homo-bimetallic bridging Co═N═Co complexes through steric and geometric control to gain access and insight into elusive cobalt−nitride bonds.

As part of our ongoing effort to utilize bulky guanidinate ligands to stabilize 3d metal complexes with rare and reactive bonding motifs,[27,28] herein we demonstrate the isolation and the reactivity studies of a midvalent, four-coordinate, bimetallic Co(III)−nitride complex, namely $[\text{Na(THF)}_4][(^{ket}\text{guan})\text{Co}(\mu\text{-N})(\text{N}_3)]_2$ (**1**) ($^{ket}$guan = ($t$Bu$_2$CN)C(NDipp)$_2$, Dipp = 2,6-diisopropylphenyl). While **1** is stable as a solid and in solution, chemical activation of the nitride moiety can be achieved by perturbation of the ligand field through a coordination switch attained by simple addition of pyridine, resulting in intermolecular hydrogen atom abstraction (HAA) chemistry. Impressively, **1** can perform HAA on strong, unactivated C−H bonds (BDE ∼ 100 kcal/mol), generating the parent−imido, mixed-valent complex $[(^{ket}\text{guan})\text{Co(py)}][(^{ket}\text{guan})\text{Co}](\mu\text{-NH})(\mu\text{-N}_3)$ (**5**). Moreover, **1** is reactive toward dihydrogen, cleaving the $H_2$ bond (BDE ∼ 105 kcal/mol) to give the parent bis(imido) $[(^{ket}\text{guan})\text{Co}(\mu\text{-NH})]_2$ (**6**).

The combined stability of **1** and its solvent-triggered nitride activation provides a unique platform and opportunity to study the chemistry of cobalt nitrides and multiply bonded late 3d metal complexes.

## RESULTS AND DISCUSSION

**Synthesis and Characterization.** Addition of K[$^{ket}$guan] to $\text{CoBr}_2$(DME) in THF affords monomeric ($^{ket}$guan)Co(Br)(THF) (**2**), which is readily converted to the cobaltate


https://dx.doi.org/10.1021/jacs.0c00291
J. Am. Chem. Soc. 2020, 142, 8233−8242

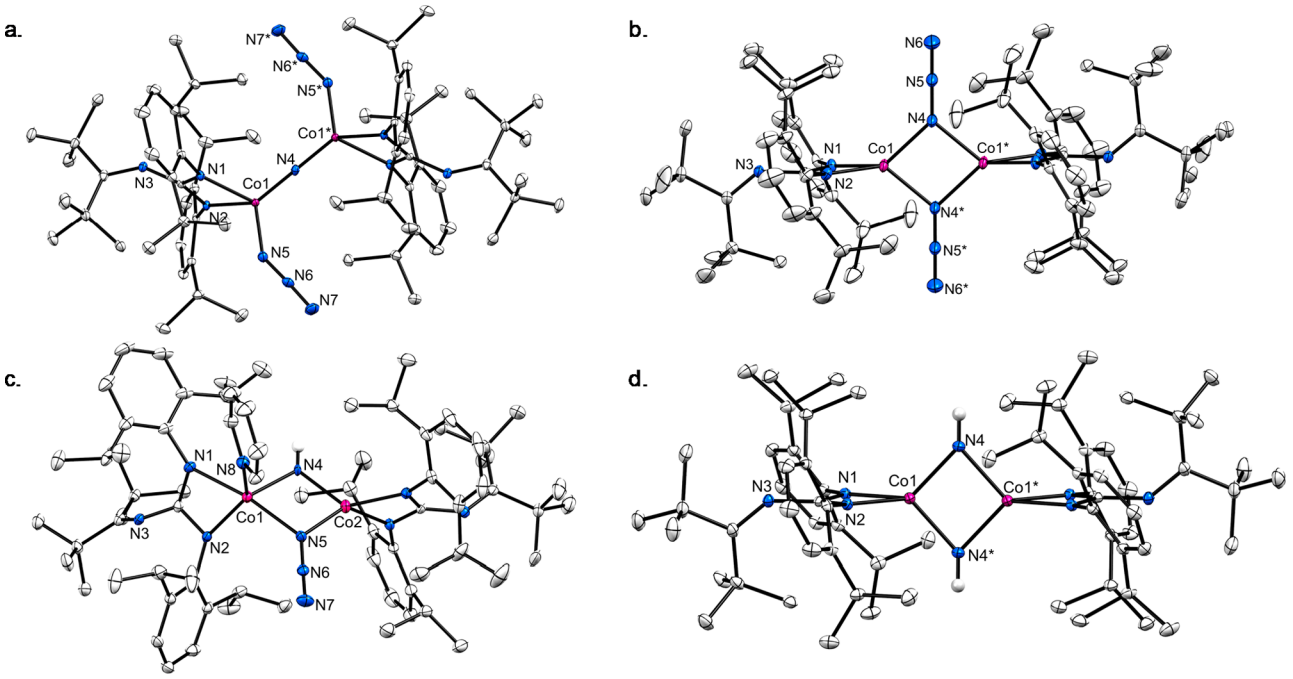


**Figure 1.** ORTEP representation of compounds (a) **1**·CHD (b) **3b**·THF (c) **5**·$C_6H_{14}$, and (d) **6**·$2C_6H_{14}$·$2C_5H_{12}$ with 30% probability ellipsoids. The $[Na(THF)_4]^+$ cation of **1**, the hydrogen atoms (exception N−H of **5** and **6**), and cocrystallized solvents are omitted for clarity. Asterisks denote symmetry-generated atoms.

bis(azide) complex $[Na(THF)_x][(^{ket}guan)Co(N_3)_2]$ (**3a**) upon treatment with excess $NaN_3$ in THF (Scheme 1). In the absence of any structural data for **3a**, it is ostensibly formulated as a monomeric species. Upon dissolution in aromatic or nonpolar solvents, the $NaN_3$ is rapidly lost to give the neutral dimer $[(^{ket}guan)Co(N_3)]_2$ (**3b**) (Scheme 1). As clearly observed through $^1H$ NMR spectroscopy, **2** and **3** are paramagnetic complexes (Figures S9−S11). While pristine samples of **3a** are complicated by the facile loss of $NaN_3$, SQUID magnetometry measurements on solid-state samples of **3b** reveal a room temperature effective magnetic moment of 7.3 $\mu_B$ (Figure S29). This value is slightly higher than expected for the spin-only value for two noninteracting high-spin Co(II) centers (5.48 $\mu_B$) but not beyond the range typically encountered for systems with high magnetic anisotropies.[29,30] Interestingly, bridging $\mu$-1,1-$N_3$ azide units are known to facilitate ferromagnetic interactions in binuclear nickel systems,[31] and a sharp rise is visible in the low-temperature region of the $\mu_{eff}$ vs $T$ and $\chi T$ vs $T$ plots for **3b** with a maximum at 7 K (9.32 $\mu_B$; 10.84 $cm^3$ K $mol^{-1}$) indicative of ferromagnetic coupling (Figure S29).[32−35]

Compound **2** is isolated as a dark blue material, whereas **3a** and **3b** are green solids, all air-sensitive but stable indefinitely under a dinitrogen atmosphere. Complex **3a** is primarily stable to $NaN_3$ loss in THF solution but typically gives mixtures of **3a** and **3b** upon attempted isolation in the solid state. Regardless, the presence of **3a** in solution is easily detected as it is spectroscopically distinct from **3b** as indicated by NMR and UV−vis spectroscopies.

Single crystals of **3b** can be grown from a saturated THF/hexanes (1:1) solution stored at −30 °C for 1 day. X-ray diffraction analysis of **3b** confirms the formation of a four-coordinate, diamond core cobalt center (Figure 1b). The molecule crystallizes in the $P2_1/c$ space group and contains one-half of the dimer in the asymmetric unit which generates the full molecule through inversion symmetry. The bond metrics of **3b** (Co1−N1 = 1.994(2) Å, Co1−N2 = 1.988(2) Å, and Co1−N4 = 1.997(2) Å) are comparable to those found in the related dinuclear cobalt complex $\{[(iPr_2N)C(NDipp)_2]$-$Co(\mu\text{-}N_3)\}_2$ (Co−N = 1.991(3) − 1.994(3) Å, $Co-N_{azide}$ = 2.010(3) Å).[36] Inspection of the azide units in **3b** reveals inequivalent N−N distances (N4−N5 = 1.227(3) Å, N5−N6 = 1.135(4) Å) consistent with azide activation,[37] a feature also present in $\{[(iPr_2N)C(NDipp)_2]Co(\mu\text{-}N_3)\}_2$.

Furthermore, treatment of **3a** with a $C_6H_6$/py (10:1) solution produces a mixture of the dimer $[(^{ket}guan)Co(N_3)$-$(py)]_2$ (**4a**) and the mononuclear $\{[Na(THF)_2][(^{ket}guan)Co$-$(py)(N_3)_2]\}n$ (**4b**) (Figures S5 and S6), with both complexes featuring five-coordinate cobalts. In the latter case, the sodium cations bridge the azide groups to give a 1D-coordination polymer. Similar solubility properties complicate separation; however, **4a** is selectively obtained from the addition of pyridine to benzene solutions of **3b**, which occurs instantaneously (Scheme 1). Of further note, the solid-state molecular structure of **4a**·THF·$C_5H_{12}$ (Figure S5) shows azide rearrangement, adopting end-on coordination modes, with the cobalt centers in distorted square-pyramidal geometries. Parkin and co-workers have found that *endo*-oriented azides, such as those in **4a**·THF·$C_5H_{12}$, are more sensitive to $N_2$ loss,[38] suggesting the end-on arrangement may be a key step in the nitride formation of **1**. Yet, poor resolution of the diffraction data only permits a qualitative structural analysis of **4a**·THF·$C_5H_{12}$, preventing assessment of azide N−N distances and their degree of activation.

Based upon the azide activation observed for **3b**, attempts were undertaken to initiate $N_2$ loss to generate cobalt nitrides. Photolyzing $C_6D_6$ solutions of **3b** leads to decomposition and formation of $^{ket}$guanH as the only identifiable product. On the other hand, room temperature photolysis (365 nm) of THF solutions of **3a** gradually gives way to the formation of a new


https://dx.doi.org/10.1021/jacs.0c00291
J. Am. Chem. Soc. 2020, 142, 8233−8242

paramagnetic species. The product is sparingly soluble and deposits as a crystalline solid from the photoreaction mixture, even when performed in dilute solutions (ca. 5 mmol). The X-ray determined solid-state molecular structure revealed the formation of the dinuclear cobalt nitride **1**·THF (Figure S2), but poor X-ray data preclude accurate parameter evaluation. Surprisingly, higher quality single crystals suitable for X-ray diffraction analysis can be obtained through photolysis of **3a** in THF solutions containing excess 1,4-cyclohexadiene (CHD) to give **1**·CHD (Scheme 1) (Figure 1a and Figure S1). The electronic absorption profiles of **1**·THF and **1**·CHD are identical by UV−vis spectroscopy (Figure S32).

It should be noted that in the solid-state, **1**·CHD forms a 1D-coordination polymer formed through bridging sodium-to-azide contacts. Addition of 18-crown-6 to suspensions of **1**·CHD or **1**·THF fails to solubilize the material.

To the best of our knowledge, **1** represents the first example of a low-nuclearity cobalt nitride complex as the closest related systems are nitride-encapsulated homo- and heterometallic clusters of the type $[Co_{10}Rh(N)_2(CO)_{21}]^{-3}$.[39] Compound **1**·CHD crystallizes in the $P\bar{1}$ space group, displaying one-half molecule in the asymmetric unit with the full dimer generated through inversion symmetry, and consequently, the Co1−N4−Co1* bond angle is perfectly linear. Examination of the crystallographically unique cobalt−nitride distance (Co1−N4 = 1.678(1) Å) shows that it falls within the typical range of cobalt−imido Co=NR distances (cf. $[(iPr_2N)C(NDipp)_2]$-Co(=NAd): Co−N = 1.621(3) Å;[36] $[(TIMEN^{aryl})Co(=NAr)](BPh_4)$: Co−N = 1.675(8) Å).[40]

The metrical parameters of **1** are suggestive of a dimer with a core $Co^{III}=N=Co^{III}$ unit. Yet, formal charge assignments can be complicated by a number of factors in molecules of this type. For example, the related Rh dimer (PNN)Rh(N·)Rh-(PNN) (PNN = 6-di(*tert*-butyl)phosphinomethylene-2,2′-bipyridine) is formulated as a Rh(II)/Rh(II) complex with a reactive, bridging nitridyl radical as discerned through electronic structure calculations.[41] However, high electron delocalization obfuscates definitive oxidation state assignments, and the rhodium dimer may be more appropriately presented as $\{Rh_2N\}^{17}$ by utilizing Enemark−Feltham notation, taking into consideration the number of nitride N-atom-based $\pi$-symmetry electrons. Extension of this notion to **1** would provide a $\{Co_2N\}^{16}$ core, where we assert the geometry and lower electron count aids in avoiding population of Co−N $\pi$*-orbitals (vide infra).

The room-temperature effective magnetic moment of **1** is 3.60 $\mu_B$ (Figure S28), substantially lower than predicted for a Co(III)/Co(III) system containing two noninteracting, $S$ = 2 ions (6.9 $\mu_B$). The lower than expected $\mu_{eff}$ can be readily explained by electron pairing through the nitride bridge (see electronic structure analysis). Moreover, the $\chi T$ vs $T$ plot slopes from 1.57 $cm^3$ K $mol^{-1}$ at 300 K to 0.08 $cm^3$ K $mol^{-1}$ at 2 K (or $\mu_{eff}$ vs $T$ from 3.60 $\mu_B$ to 0.82 $\mu_B$, respectively) (Figure S28), indicating increased antiferromagnetic coupling to a singlet ground state at low temperature. Interestingly, a small peak with a local maxima value of 0.23 $cm^3$ K $mol^{-1}$ appears in the $\chi T$ vs $T$ plot at 13 K (Figure S28). The reproducibility of this feature in both zero-field-cooled (ZFC) and field-cooled (FC) magnetization measurements indicates that this is a magnetic transition associated with the onset of ferromagnetic coupling, not unlike that observed for **3b**. Indeed, mixed antiferromagnetic and ferromagnetic coupling has been noted for other multimetallic 3d metal systems.[42−46]

The groups of Holland and Betley have demonstrated that geometric perturbation of the three-coordinate Fe(III) and Co(III) imidos $L^{Me}Fe(NAd)$ ($L^{Me}$ = 2,4-bis(DippN)pent-3-yl) and ($^{dipy}$L)Co(NR) ($^{dipy}$L = 5-mesityl-1,9-(2,4,6-$Ph_3C_6H_2$)-dipyrrin), respectively, by pyridine ligation to give tetrahedral (L)M(NR)(py) leads to ligand-accelerated C−H bond amination chemistry.[47,48] Enhanced reactivity toward C−H bonds in the presence of pyridine with the (salen)ruthenium-(VI)−nitride complex [(salen)Ru-(N)(MeOH)]$PF_6$ has also been reported.[49] In these cases, reactivity promotion is ascribed in part to coordination dependent, spin-state changes that lead to the population of M−N $\pi$*-orbitals upon pyridine binding.[47,48]

Upon investigation of the role of pyridine coordination in our system, addition of pyridine to **1**·CHD leads to the quantitative formation of the bimetallic bridging imido [($^{ket}$guan)Co(py)][($^{ket}$guan)Co]($\mu$-NH)($\mu$-$N_3$) (**5**) where its N−H proton is derived as the product of HAA from the cocrystallized CHD (eq 1). Accordingly, this reaction is

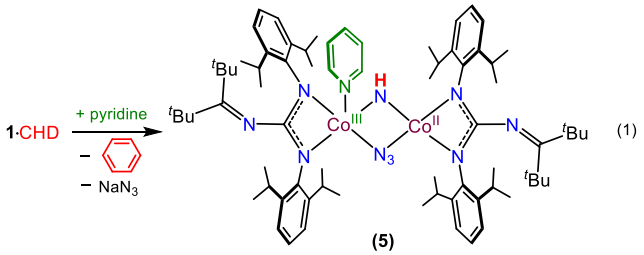


accompanied by the formation of benzene as revealed by $^1$H NMR spectroscopy (Figure S36). Compound **5** does form upon addition of pyridine to **1**·THF; however, the product mixture is marked by the presence of significant amounts of $^{ket}$guanH. Similarly, photolysis of **4a** in $C_6H_6$/py (10:1) solution also generates **5**; though, when conducted in the absence of H atom donors such as CHD, the yield is considerably lower and is also accompanied by substantial amounts of protonated $^{ket}$guanH. Moreover, photolyzing $C_6H_6$/py (10:1) solutions of the isotopomer **4a-$^{15}$N** (made with 98% enriched $Na^{15}N^{14}N^{14}N$) in the presence of excess CHD gives a 50:50 mixture of [($^{ket}$guan)Co]$_2$($\mu$-$^{14}$NH)-($\mu$-$^{15}$NNN) (**5-$^{14}$NH**) and [($^{ket}$guan)Co]$_2$($\mu$-$^{15}$NH)-($\mu$-$^{15}$NNN) (**5-$^{15}$NH**) which show respective $^{14}$N−H and $^{15}$N−H stretching frequencies of 3418 and 3400 $cm^{-1}$ in the infrared spectrum (KBr pellet) (Figure S24).

Complex **5** is a dark brown, paramagnetic compound that is soluble in nonpolar solvents. Single crystals of **5**·$C_6H_{14}$ are obtained from concentrated hexanes solution, and its solid-state molecular structure (Figure 1c) reveals an asymmetric, bimetallic complex with four- and five-coordinate cobalt centers possessing bridging NH and $N_3$ groups. The cobalt−imido bond distances of **5**·$C_6H_{14}$ (Co1−N4 = 1.963(3) Å, Co2−N4 = 1.925(3) Å) are not informative as they fall within the range of both amido (cf. $\{[(NH_2CH_2CH_2NH_2)_2Co]_2(\mu$-$NH_2)(\mu$-OH)$\}[NO_3]_4$: Co−N = 1.947(5)−1.948(5) Å)[50] and imido-bridged cobalt compounds (cf. $\{[HC(MeCNDipp)]_2Co(\mu$-NAr)$\}_2$: Co−N = 1.983(3)−1.988(3) Å).[51]

SQUID magnetometry measurements of **5** give a room temperature effective magnetic moment of 3.97 $\mu_B$. This value is considerably lower than expected for two noninteracting high-spin Co(II) ($S$ = 1.5) and Co(III) ($S$ = 2) centers (6.24


https://dx.doi.org/10.1021/jacs.0c00291
J. Am. Chem. Soc. 2020, 142, 8233−8242

$\mu_B$) but reasonable if partial antiferromagnetic interactions are present. Accordingly, the $\chi T$ vs $T$ plot is also observed to slope, dropping from 1.99 $cm^3$ K $mol^{-1}$ at 300 K to 0.42 $cm^3$ K $mol^{-1}$ at 2 K (or $\mu_{eff}$ vs $T$ from 3.97 to 1.81 $\mu_B$, respectively) (Figure S30), consistent with increased antiferromagnetic coupling to a $S$ = 0.5 ground state (calcd 0.37 $cm^3$ K $mol^{-1}$ or 1.73 $\mu_B$) at low temperature. Notably, a small, ZFC/FC-independent peak is also observed at low temperature, appearing at 18.5 K (1.00 $cm^3$ K $mol^{-1}$), indicating ferromagnetic contributions as seen with **1** and **3b**.

As in the cases of $L^{Me}Fe(NAd)$,[47] ($^{dipy}L$)Co(NR),[48] and [(salen)Ru(N)(MeOH)]$PF_6$,[49] the addition of pyridine to **1** clearly engages new reactivity where the coordinating base acts as a solvent switch to greatly enhance the reactivity of the bridging nitride atom. On the basis of our electronic structure analysis of **1** (vide infra) and the above-mentioned examples, we contend that pyridine binding leads to a spin-state promotion resulting in population of Co−N−Co $\pi^*$-orbitals. Attempts to identify a [Co(N·)Co(py)] intermediate by EPR spectroscopy via addition of pyridine to solutions of **1** were unsuccessful.

Expanding upon the observed pyridine promoted HAA chemistry of **1** toward CHD, its reactivity with other hydrocarbons was studied. Interestingly, addition of pyridine to **1** or photolysis of **4a** in $C_6H_6$/py in the presence of 9,10-dihydroanthracene (DHA) (BDE: 76.3 kcal/mol)[52] fails to give anthracene. We presume this is a consequence of steric hindrance as the two hydrocarbon substrates possess comparably weak C−H bonds (Figure 2a). A similar steric argument was invoked to explain the unreactivity of $L^{Me}Fe$-(NAd)(py) toward DHA.[47]

Conversely, **1**·THF is reactive in $C_6H_6$/py solution toward several hydrocarbon substrates, including those with strong C−H bonds, giving **5** as the sole product in nearly quantitative yields. Similarly, photolysis of **4a** in $C_6H_6$/py solution with the same hydrocarbon substrates generates **5** in equivalent yield. In particular, HAA is observed with cyclohexene (BDE: 87 kcal/mol) and fully saturated cyclohexane (BDE: 99 kcal/mol) (Figure 2a), yielding primarily benzene but also bicyclohexenyl and 1,4-cyclohexadiene in 78:17:5 and 85:8:4 ratios, respectively, as indicated by GC/MS analysis of the product mixtures (Table S4).

Notably, dissolution of **1**·THF in py-$d_5$/cyclohexane-$d_{12}$ solution yields the deuterated parent imido [($^{ket}$guan)Co-(py)][($^{ket}$guan)Co]($\mu$-ND)($\mu$-$N_3$) (**5-D**) that exhibits an N−D stretching frequency in the infrared spectrum at 2248 $cm^{-1}$ (Figure S23), within the expected isotopic mass shift range of ca. 2500 $cm^{-1}$ as compared to **5-H** ($\upsilon_{N-H}$ = 3424 $cm^{-1}$). This result is important as it corroborates an intermolecular HAA mechanism, eliminating the ligand as the H atom source.

Interestingly, performing the reaction in the presence of excess cyclooctane (BDE: 95 kcal/mol)[52] generates 1,5-cyclooctadiene almost exclusively with a trace amount of cyclooctene in a 97:2 ratio (Figure S45 and Table S4). In our studies of the HAA chemistry, we do not observe reactivity with benzene (BDE: 112.4 kcal/mol), pegging the upper limit of the C−H bond abstraction between 99.5 and 112.4 kcal/mol.

The reactivity of our system toward cyclohexane afforded us the opportunity to easily examine the KIE upon switching from $C_6H_{12}$ to $C_6D_{12}$ in the reaction mixtures. Photolysis of **4a** (100 $\mu$M) in $C_6H_6$/py (10:1) in the presence of 100 equiv of cyclohexane was followed by UV−vis absorption spectroscopy

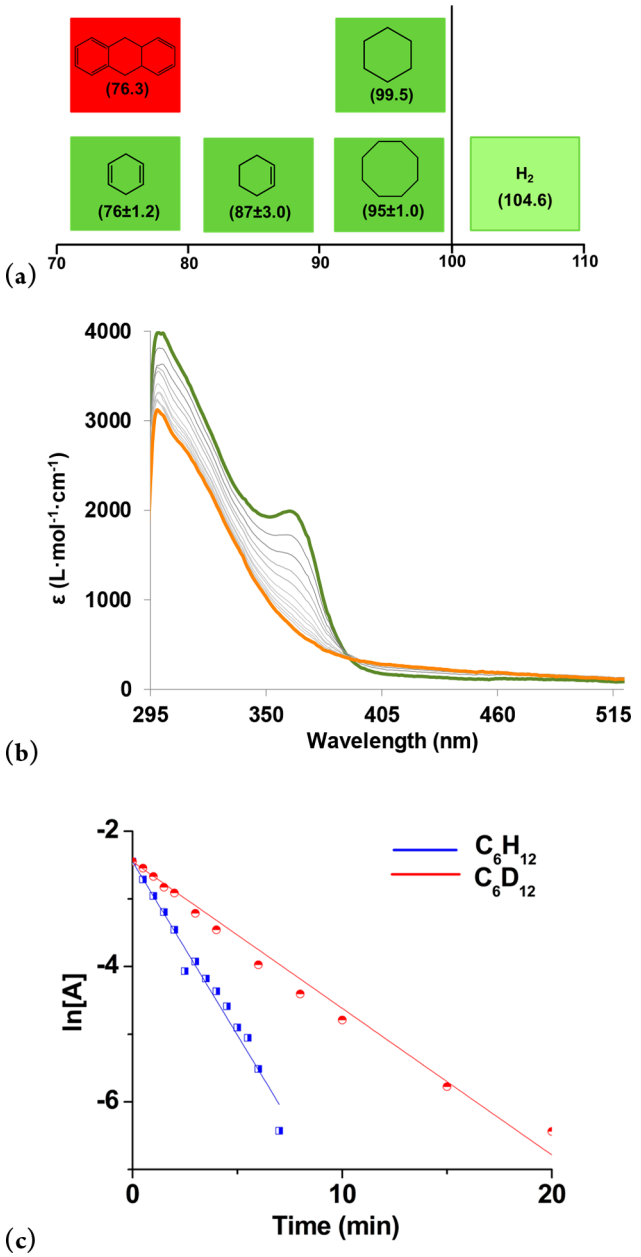


**Figure 2.** (a) Substrate screening for the HAA chemistry of **1** and respective C−H BDEs. (b) UV−vis spectra of the photoconversion of **4a** (green) to **5** (orange) in $C_6H_6$/py solution in the presence of excess CHD. (c) KIE rate plot of the photolysis of **4a** in $C_6H_6$/py (10:1) in the presence of 100 equiv of $C_6H_{12}$ (blue) and $C_6D_{12}$ (red).

(Figure 2b). As seen from the rate plot presented in Figure 2c, there is a clear difference in rate with a KIE = 2.5 ± 0.1. This value is within the KIE range established for the related Fe=O mediated HAA reactions (KIE = 2.5−5.7)[53] and in complete accordance with the HAA chemistry observed for the Co=O complex $[(N_4Py)Co(O)]^{2+}$ ($N_4Py$ = *N*,*N*-bis(2-pyridylmethyl)-*N*-bis(2-pyridyl)methylamine) (KIE = 2.1 ± 0.1).[54] This reaction can be performed on a preparative scale, giving the isotopomers **5-H** and **5-D** (Figure S23).

Understanding the reactivity of molecular metal nitrides toward hydrogen is very important for providing chemical insights into the formation of ammonia through the Haber−Bosch process.[55] Despite this, only a few examples of nitride reactivity toward $H_2$ have been reported,[8,19,56−59] with the


https://dx.doi.org/10.1021/jacs.0c00291
J. Am. Chem. Soc. 2020, 142, 8233−8242

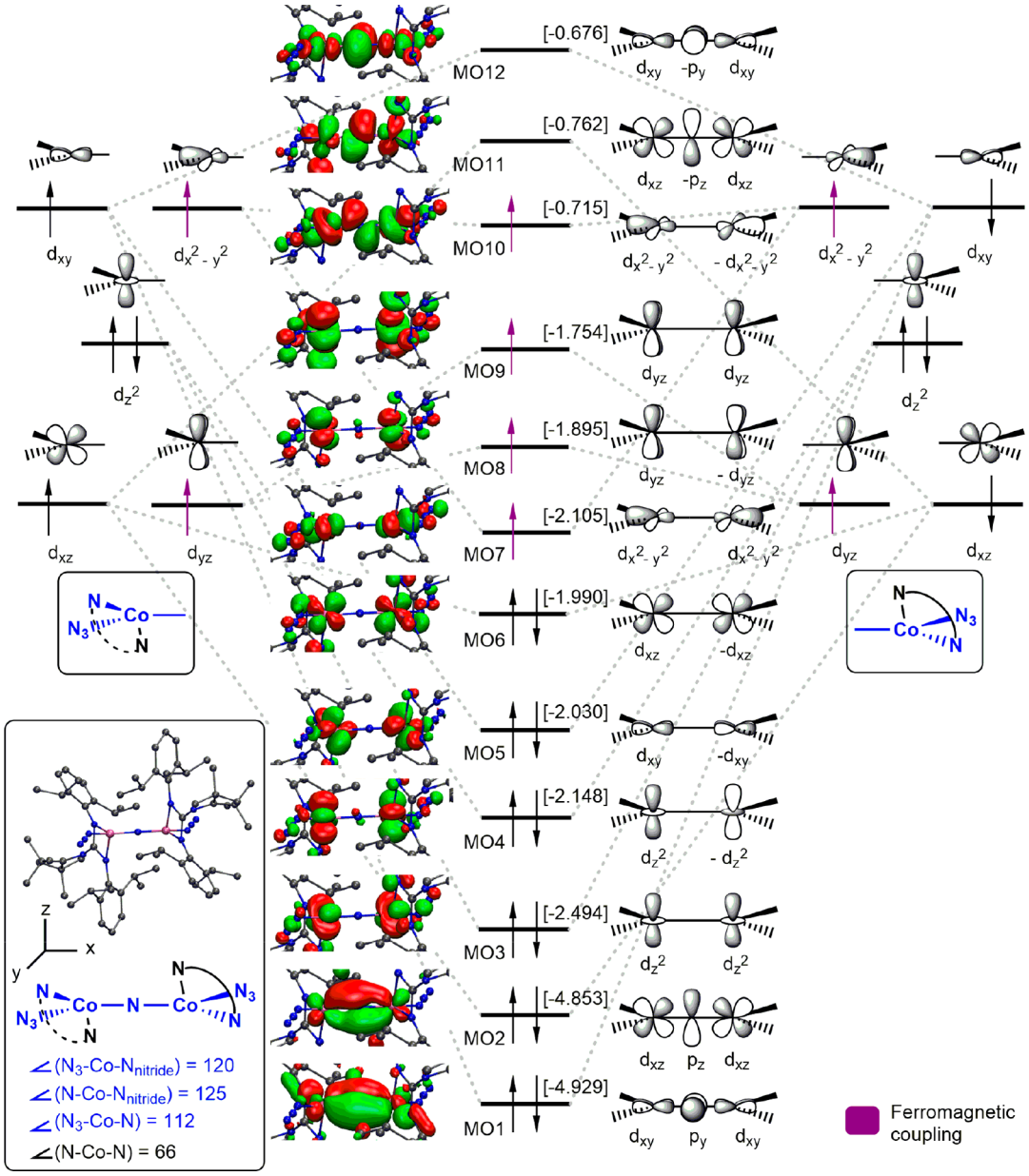


**Figure 3.** Molecular orbital diagram of the Co−N−Co core of $\mathbf{1}^{Q}$.

majority using terminal nitride species. To date, only the bimetallic nitride complexes $(L_3)Fe(\mu\text{-}N)Fe(L_3)$ ($L_3$ = $[PhB(CH_2PPh_2)_3]^-$) and $\{Cs[U(OSi(OtBu)_3)_3]_2(\mu\text{-}N)\}$ have been shown capable of heterolytically cleaving dihydrogen to give bridging $M_2(\mu\text{-}NH)(\mu\text{-}H)$ products.[56,59]

In light of the observed HAA reactivity of our dicobalt nitride, its reactivity toward $H_2$ was investigated. Suspensions of **1**·THF in a mixture of benzene and pyridine under $H_2$ (150 psi) gradually give way to a new paramagnetic product. Solutions of **4a** in $C_6H_6$/py mixtures are unreactive toward $H_2$ (150 psi); however, upon exposure to UV light, the solution gradually changes from emerald green to dark green concomitant with the formation of the same paramagnetic product after 3 days. In either case, starting with **1** or **4a**, the conversion is nearly quantitative by NMR spectroscopy. The product crystallizes from hexane/pentane solution or concentrated THF stored at −30 °C to give the parent bis(imido) $[(^{ket}guan)Co(\mu\text{-}NH)]_2$ (**6**) (Scheme 1) as the solvates **6**·$2C_6H_{14}$·$2C_5H_{12}$ and **6**·4THF, respectively.

X-ray crystallographic analysis of **6**·$2C_6H_{14}$·$2C_5H_{12}$ (Figure 1d) shows the compound crystallizes in the $P\bar{1}$ space group with three independent half-molecules in the asymmetric unit, providing the complete dimers upon symmetry generation. The metrical parameters between the monomers in the asymmetric unit are nearly identical and reveal the cobalt−imido distances to range from Co−N = 1.982(2)−1.996(2) Å, only slightly longer than those found in **5**·$C_6H_{14}$. The room temperature effective magnetic moment of **6**·4THF is 3.20 $\mu_B$, similar to that found for **1**, thus supporting a Co(III)/Co(III) assignment for **6** possessing partial antiferromagnetic coupling contributions. Indicative of such, the $\chi T$ vs $T$ plot decreases in a near linear fashion from 1.25 $cm^3$ K $mol^{-1}$ at 300 K to 0.04 $cm^3$ K $mol^{-1}$ at 2 K (Figure S31). Yet, as **6** is lacking bridging azide groups, no ferromagnetic coupling features are observed at low temperatures as seen with **1**, **3b**, and **5**.


https://dx.doi.org/10.1021/jacs.0c00291
J. Am. Chem. Soc. 2020, 142, 8233−8242

Following the formation of **6** by $^1$H NMR spectroscopy shows nearly quantitative conversion, and the product is isolated in 73% yield. Whether **6** forms from the heterolytic or homolytic cleavage of $H_2$ is not known at this time, though the preference in our system for HAA of strong C−H bonds suggests the latter. Conducting the experiment in $C_6D_6$/py-$d_5$ with $H_2$ exclusively gives **6-H** with a N−H stretching frequency appearing at 3422 $cm^{-1}$ (Figure S25), indicating no HAA reactivity with the solvent. Conversely, performing the identical experiment in $C_6H_6$/py-$h_5$ under a $D_2$ atmosphere leads to the exclusive formation of the deuterium isotopomer $[(^{ket}guan)Co(\mu\text{-ND})]_2$ (**6-D**) as indicated by IR spectroscopy ($\nu_{N-D}$ = 2318 $cm^{-1}$) (Figure S27), further eliminating the solvent or ligand as the hydrogen atom sources. Finally, photolyzing $C_6D_6$/py-$d_5$ solutions of **5** under $H_2$ (150 psi) gradually gives way to **6**, suggesting the formation of the bis(imido) occurs stepwise.

**Computed Geometry and Electronic Structure.** To scrutinize the electronic structure of **1**, we turned to density functional theory (DFT). Using a nontruncated model of **1**, in an anionic form without the $[Na(THF)_4]^+$ counterion, the empirical X-ray structure was remarkably reproduced by dispersion-corrected DFT calculations in the quintet spin state (see the Supporting Information for details). This quintet ($\mathbf{1}^{Q}$), with two unpaired electrons at each cobalt center, agrees with the measured $\mu_{eff}$ = 3.60 $\mu_B$ at room temperature. A broken-symmetry single state was found to be more stable by 22.64 kcal/mol than the quintet, and accordingly, it represents the ground state of **1** at 0 K ($\mathbf{1}^{S}$). As pure functionals, like the PBE used, have the tendency to overstabilize low spin states, the quintet state is plausibly much closer in energy to an antiferromagnetically derived singlet than predicted by DFT. The structural parameters of $\mathbf{1}^{S}$ are similar to $\mathbf{1}^{Q}$, except the Co−N−Co angle becomes slightly bent at 162°, which facilitates the antiferromagnetic coupling of the metal-centered radicals through the nitride center.

Clearly, the quintet state description is most pertinent as it best represents the observed character of **1**. Thus, we used quasi-restricted orbitals (QROs) (Figure 3) to rationalize and characterize the electronic structure of $\mathbf{1}^{Q}$. QROs express unrestricted wave functions (with different $\alpha$ and $\beta$ orbital subsets) through the intuitive conceptual picture of the restricted open-shell (RO) solution with doubly and singly occupied orbitals (i.e., through identical $\alpha$ and $\beta$ spatial orbitals).

According to the features of the revealed molecular QROs, $\mathbf{1}^{Q}$ can be formally described as possessing two high-spin Co(III) centers exhibiting both antiferromagnetic and weak ferromagnetic coupling through two two-electron interactions (Figure 3). In particular, the formal partition of these delocalized MOs to individual cobalt contributions gives four half-filled d-orbitals, $d_{xz}$, $d_{yz}$, $d_{xy}$, and $d_{x^2-y^2}$, with a doubly occupied $d_{z^2}$-orbital at each metal. At each cobalt, two of the metal-centered radicals pair through the $\pi$-subspace (MO5 and MO6 in Figure 3), whereas the couplings of unpaired electrons with local $\sigma$- and $\delta$-symmetries through the nitrogen remain weak and ferromagnetic in nature (MO7−MO10 in Figure 3).

To better envisage the bonding interactions in $\mathbf{1}^{Q}$, a simplified substructure of the "$(^{ket}guan)Co(\mu\text{-N})(N_3)$" unit can be defined by the cobalt center, its azide group, the bridging $N_{nitride}$, and one of the nitrogen contact atoms from each $[^{ket}guan]^-$ ligand, giving an $ML_3$ structural approximation for each metal which is highlighted in blue in Figure 3 (see the inset). This yields a planar arrangement where the ligand atoms are separated by nearly 120°, affording a $D_{3h}$ symmetry approximation for each cobalt fragment with the out-of-plane nitrogen atom of the $[^{ket}guan]^-$ ligand acting as an asymmetric axial perturbation on the idealized electronic structure at the metal. Through this perspective, the d-orbital arrangement represents the most ideal orientation for the schematic representation of the cobalt−nitride and cobalt−cobalt interactions.

Therefore, the in-plane $Co(d_{xy})$ orbitals are perfectly oriented on both sides to form an appreciable three-center interaction with the $p_y$ orbital of the $N_{nitride}$ atom as seen in the molecular orbital picture, MO1, in Figure 3. An almost identical three-center $\pi$-interaction (MO2) evolves in the perpendicular $xz$-plane through the $Co(d_{xz})$ + $N(p_z)$ + $Co(d_{xz})$ atomic orbital combination. Both of these molecular orbitals formally represent $N_{nitride}$-based lone pairs; however, the spatial distributions clearly expose delocalization to the metals, resulting in the formation of $\pi$-type bonding interactions of covalent character. The two other lone pairs of the formally $N^{3-}$ bridge are represented by low-lying orbitals with $N(p_x)$ and N(s) character (not shown in Figure 3). The $\pi$ interactions along the Co−N−Co axis are, in fact, classical three-center, four-electron interactions, giving way to the $Co(d_{xy})$−$Co(d_{xy})$ (MO5) and $Co(d_{xz})$−$Co(d_{xz})$ (MO6) antisymmetric nonbonding, metal-centered orbital combinations (Figure 3). Being doubly occupied, MO5 and MO6 represent the $\pi$-subspace, d-electron pairing.

In the $\sigma$-subspace, the $Co(d_{x^2-y^2})$ orbitals are arranged with the N(s) orbital to form a direct Co−N−Co $\sigma$-interaction, leading to a low-lying orbital combination (not depicted in Figure 3). Along these lines, the $Co(d_{x^2-y^2})$ + $N(p_x)$ + $Co(d_{x^2-y^2})$ and $Co(d_{x^2-y^2})$−$N(p_x)$−$Co(d_{x^2-y^2})$ arrangements also leads to appreciable $\sigma$- and $\sigma^*$-combinations; though, $Co(d_{x^2-y^2})/(p_x)$ orbital hybridizations give rise to the predominantly nonbonding, metal-based combinations MO7 and MO10 (Figure 3). Together with the symmetric and antisymmetric $\delta$-symmetry oriented d-orbital combinations, $Co(d_{yz})$ + $Co(d_{yz})$ and $Co(d_{yz})$−$Co(d_{yz})$, respectively, with practically zero overlap, the $\sigma$- and $\delta$-symmetry d-orbitals appear as quasi-degenerate orbitals (MO7−MO10) with each hosting one electron according to Hund's maximum multiplicity rule.

Owing to the strong delocalization of the nitride lone pairs to the metals (MO1 and MO2), the central Co−N interactions have a notable $\pi$-bond character in addition to the dative $\sigma$-bond. Accordingly, the electronic structure of $\mathbf{1}^{Q}$ can be best represented by the $Co^{III}$=N=$Co^{III}$ canonical form, with the data indicating no radical character at the nitride atom. Mayer bond orders of 1.33 calculated for the Co−N interactions support this notion. The spin density value of 1.5 at each cobalt also conforms to the partial paring of the d-electrons. As the unpaired electrons occupy $\sigma$- and $\delta$-symmetry metal orbitals that cannot mix with the nitrogen's $\pi$-symmetry $p_x$ and $p_z$ atomic orbitals, the radical character cannot delocalize to the bridging nitrogen, which is reflected by the negligible atom-condensed spin density value of 0.1 at the nitrogen.

The lowest-lying unoccupied molecular orbitals, MO11 and MO12, correspond to the antibonding combinations of the Co=N=Co $\pi$-interactions and have notable amplitude at the central nitrogen due to the covalent nature of the Co−N $\pi$-bonds. In comparison, the reported spin density distribution of the related dimer (PNN)Rh(N·)Rh(PNN)[15] closely resembles


https://dx.doi.org/10.1021/jacs.0c00291
J. Am. Chem. Soc. 2020, 142, 8233−8242

the out-of-plane antibonding combination of $\mathbf{1}^{Q}$, MO11, with one electron occupancy of this orbital in the dirhodium nitride case. As a matter of fact, this additional electron within the $\{Rh_2N\}^{17}$ core of (PNN)Rh(N·)Rh(PNN) embodies the most significant formal difference between its electronic structure and the $\{Co_2N\}^{16}$ core of $\mathbf{1}^{Q}$, thus giving way to the observed nitridyl radical character in (PNN)Rh(N·)Rh(PNN) that is absent in $\mathbf{1}^{Q}$.

## CONCLUSION

In conclusion, while late metal complexes of the type M═E/M≡E can be difficult to access and stabilize because of "oxo wall" considerations, we show here that surrogates for such chemistry can be obtained through systems of the type M═E═M. In this case, we demonstrate that the first example of a bimetallic cobalt nitride, compound **1**, is accessed through photolysis of a guanidinate cobalt−azide precursor. According to DFT calculations, conforming also to experimental observations, the calculated quintet $\mathbf{1}^{Q}$ possesses two high-spin cobalt(III) centers coupled through a formal $Co^{III}$═N═$Co^{III}$ core with covalent Co−N $\pi$-bonds. The pseudoplanar arrangement about the $Co^{III}$═N═$Co^{III}$ unit facilitates the pairing of $\pi$-symmetry metal-centered radicals (two at each Co) across the bridging nitride, whereas the inefficient through-space interaction of $\sigma$- and $\delta$-symmetry d-orbitals leads to the weak ferromagnetic coupling of the corresponding unpaired electrons (also two at each Co), eventuating in an $S$ = 2, quintet spin state of $\mathbf{1}^{Q}$. The geometry and electron count of the cobalt centers avoid population of Co−N $\pi$*-orbitals, thereby avoiding radical character at the N atom. Consequently, **1** is stable in solution and as a solid. However, its N atom reactivity is accessible through addition of pyridine, triggering HAA chemistry to give the bridged imido **5**. Impressively, this HAA reactivity extends to strong C−H bonds such as those found in cyclohexane (BDE ∼ 100 kcal/mol). Moreover, this chemistry can be further extended to include $H_2$, leading to a rare example of hydrogen activation by a molecular metal nitride to generate the bis(imido) **6**. At present, investigations are underway to understand the observed $H_2$ activation chemistry while working to apply our synthetic strategy to other late metal systems.

## ASSOCIATED CONTENT

### Supporting Information

The Supporting Information is available free of charge at https://pubs.acs.org/doi/10.1021/jacs.0c00291.

Experimental procedures, spectral data for all the complexes, magnetic data, and computational details (PDF)

Crystallographic details of **1**·CHD (CIF)

Crystallographic details of **2** (CIF)

Crystallographic details of **3b**·THF (CIF)

Crystallographic details of **5**·$C_6H_{14}$ (CIF)

Crystallographic details of **6**·2$C_6H_{14}$·2$C_5H_{12}$ (CIF)

## AUTHOR INFORMATION


### Corresponding Authors

**Skye Fortier** − *Department of Chemistry and Biochemistry, University of Texas at El Paso, El Paso, Texas 79968, United States;* orcid.org/0000-0002-0502-5229; Email: asfortier@utep.edu

**Balazs Pinter** − *Department of Chemistry, Universidad Técnica Federico Santa Maria, 2390123, Chile;* orcid.org/0000-0002-0051-5229; Email: balazs.pinter@usm.cl

### Authors

**Debabrata Sengupta** − *Department of Chemistry and Biochemistry, University of Texas at El Paso, El Paso, Texas 79968, United States;* orcid.org/0000-0001-7212-3761

**Christian Sandoval-Pauker** − *Department of Chemistry, Universidad Técnica Federico Santa Maria, 2390123, Chile;* orcid.org/0000-0002-7831-331X

**Emily Schueller** − *Materials Department and Materials Research Laboratory, University of California, Santa Barbara, Santa Barbara, California 93106, United States;* orcid.org/0000-0002-7108-7399

**Angela M. Encerrado-Manriquez** − *Department of Chemistry and Biochemistry, University of Texas at El Paso, El Paso, Texas 79968, United States;* orcid.org/0000-0002-9822-3549

**Alejandro Metta-Magaña** − *Department of Chemistry and Biochemistry, University of Texas at El Paso, El Paso, Texas 79968, United States;* orcid.org/0000-0001-9993-8485

**Wen-Yee Lee** − *Department of Chemistry and Biochemistry, University of Texas at El Paso, El Paso, Texas 79968, United States*

**Ram Seshadri** − *Materials Department and Materials Research Laboratory and Department of Chemistry and Biochemistry, University of California, Santa Barbara, Santa Barbara, California 93106, United States;* orcid.org/0000-0001-5858-4027

Complete contact information is available at: https://pubs.acs.org/10.1021/jacs.0c00291


### Notes

The authors declare no competing financial interest.

## ACKNOWLEDGMENTS

We are grateful to the NSF (CHE-1664938 and DMR-1827745; S.F.) and the Welch Foundation (AH-1922-20170325; S.F) for financial support of this work. S.F. is an Alfred P. Sloan Foundation research fellow and is thankful for their support. We also acknowledge the NSF-MRI program (CHE-1827875) for providing funding for the purchase of an X-ray diffractometer. Magnetic measurements were performed at the shared experimental facilities of the NSF Materials Research Science and Engineering Center (MRSEC) at UC Santa Barbara (DMR 1720256). The UCSB MRSEC is a member of the NSF-supported Materials Research Facilities Network (www.mrfn.org).

## REFERENCES

(1) Hohenberger, J.; Ray, K.; Meyer, K. The biology and chemistry of high-valent iron-oxo and iron-nitrido complexes. *Nat. Commun.* **2012**, *3*, 720.

(2) Grubbs, R. H.; Wenzel, A. G.; O'Leary, D. J.; Khosravi, E. *Handbook of Metathesis*; Wiley-VCH Verlag GmbH & Co.: Weinheim, Germany, 2015.

(3) Schrock, R. R. Multiple metal-carbon bonds for catalytic metathesis reactions (Nobel Lecture). *Angew. Chem., Int. Ed.* **2006**, *45* (23), 3748−3759.

(4) Smith, J. M. Reactive transition metal nitride complexes. *Prog. Inorg. Chem.* **2014**, *58*, 417−470.

(5) Gray, H. B.; Winkler, J. R. Living with Oxygen. *Acc. Chem. Res.* **2018**, *51* (8), 1850−1857.

(6) Berry, J. F. Terminal nitrido and imido complexes of the late transition metals. *Comments Inorg. Chem.* **2009**, *30* (1−2), 28−66.
(7) Hartmann, N. J.; Wu, G.; Hayton, T. W. Synthesis of a "Masked" Terminal Nickel(II) Sulfide by Reductive Deprotection and its Reaction with Nitrous Oxide. *Angew. Chem., Int. Ed.* **2015**, *54* (49), 14956−14959.
(8) Scheibel, M. G.; Askevold, B.; Heinemann, F. W.; Reijerse, E. J.; de Bruin, B.; Schneider, S. Closed-shell and open-shell square-planar iridium nitrido complexes. *Nat. Chem.* **2012**, *4* (7), 552−558.
(9) O'Halloran, K. P.; Zhao, C. C.; Ando, N. S.; Schultz, A. J.; Koetzle, T. F.; Piccoli, P. M. B.; Hedman, B.; Hodgson, K. O.; Bobyr, E.; Kirk, M. L.; Knottenbelt, S.; Depperman, E. C.; Stein, B.; Anderson, T. M.; Cao, R.; Geletii, Y. V.; Hardcastle, K. I.; Musaev, D. G.; Neiwert, W. A.; Fang, X. K.; Morokuma, K.; Wu, S. X.; Kogerler, P.; Hill, C. L. Revisiting the Polyoxometalate-Based Late-Transition-Metal-Oxo Complexes: The "Oxo Wall" Stands. *Inorg. Chem.* **2012**, *51* (13), 7025−7031.
(10) Winkler, J. R.; Gray, H. B. Electronic structures of oxo-metal ions. *Struct. Bonding (Berlin)* **2011**, *142*, 17−28.
(11) Schoffel, J.; Susnjar, N.; Nuckel, S.; Sieh, D.; Burger, P. 4d vs. 5d-Reactivity and Fate of Terminal Nitrido Complexes of Rhodium and Iridium. *Eur. J. Inorg. Chem.* **2010**, *2010* (31), 4911−4915.
(12) Rebreyend, C.; Mouarrawis, V.; Siegler, M. A.; van der Vlugt, J. I.; de Bruin, B. Steric Protection of Rhodium-Nitridyl Radical Species. *Eur. J. Inorg. Chem.* **2019**, *2019* (39−40), 4249−4255.
(13) Saouma, C. T.; Peters, J. C. M E and M = E complexes of iron and cobalt that emphasize three-fold symmetry (E O, N, NR). *Coord. Chem. Rev.* **2011**, *255* (7−8), 920−937.
(14) Hay-Motherwell, R. S.; Wilkinson, G.; Hussain-Bates, B.; Hursthouse, M. B. Synthesis and x-ray crystal structure of oxotrimesityliridium(V). *Polyhedron* **1993**, *12* (16), 2009−12.
(15) Gloaguen, Y.; Rebreyend, C.; Lutz, M.; Kumar, P.; Huber, M.; van der Vlugt, J. I.; Schneider, S.; de Bruin, B. An Isolated Nitridyl Radical-Bridged {Rh(N.)Rh} Complex. *Angew. Chem., Int. Ed.* **2014**, *53* (26), 6814−6818.
(16) Scheibel, M. G.; Wu, Y.; Stueckl, A. C.; Krause, L.; Carl, E.; Stalke, D.; de Bruin, B.; Schneider, S. Synthesis and Reactivity of a Transient, Terminal Nitrido Complex of Rhodium. *J. Am. Chem. Soc.* **2013**, *135* (47), 17719−17722.
(17) Angersbach-Bludau, F.; Schulz, C.; Schoeffel, J.; Burger, P. Syntheses and electronic structures of $\mu$-nitrido bridged pyridine, diimine iridium complexes. *Chem. Commun. (Cambridge, U. K.)* **2014**, *50* (63), 8735−8738.
(18) Schoeffel, J.; Rogachev, A. Y.; DeBeer George, S.; Burger, P. Isolation and Hydrogenation of a Complex with a Terminal Iridium-Nitrido Bond. *Angew. Chem., Int. Ed.* **2009**, *48* (26), 4734−4738.
(19) Schoffel, J.; Rogachev, A. Y.; George, S. D.; Burger, P. Isolation and Hydrogenation of a Complex with a Terminal Iridium-Nitrido Bond. *Angew. Chem., Int. Ed.* **2009**, *48* (26), 4734−4738.
(20) Sieh, D.; Schlimm, M.; Andernach, L.; Angersbach, F.; Nuckel, S.; Schoffel, J.; Susnjar, N.; Burger, P. Metal-Ligand Electron Transfer in 4d and 5d Group 9 Transition Metal Complexes with Pyridine, Diimine Ligands. *Eur. J. Inorg. Chem.* **2012**, *2012* (3), 444−462.
(21) Goetz, M. K.; Hill, E. A.; Filatov, A. S.; Anderson, J. S. Isolation of a Terminal Co(III)-Oxo Complex. *J. Am. Chem. Soc.* **2018**, *140* (41), 13176−13180.
(22) Hojilla Atienza, C. C.; Bowman, A. C.; Lobkovsky, E.; Chirik, P. J. Photolysis and Thermolysis of Bis(imino)pyridine Cobalt Azides: C-H Activation from Putative Cobalt Nitrido Complexes. *J. Am. Chem. Soc.* **2010**, *132* (46), 16343−16345.
(23) Zolnhofer, E. M.; Kaess, M.; Khusniyarov, M. M.; Heinemann, F. W.; Maron, L.; van Gastel, M.; Bill, E.; Meyer, K. An Intermediate Cobalt(IV) Nitrido Complex and its N-Migratory Insertion Product. *J. Am. Chem. Soc.* **2014**, *136* (42), 15072−15078.
(24) Hong, S.; Pfaff, F. F.; Kwon, E.; Wang, Y.; Seo, M.-S.; Bill, E.; Ray, K.; Nam, W. Spectroscopic Capture and Reactivity of a Low-Spin Cobalt(IV)-Oxo Complex Stabilized by Binding Redox-Inactive Metal Ions. *Angew. Chem., Int. Ed.* **2014**, *53* (39), 10403−10407.
(25) Wang, B.; Lee, Y.-M.; Tcho, W.-Y.; Tussupbayev, S.; Kim, S.-T.; Kim, Y.; Seo, M. S.; Cho, K.-B.; Dede, Y.; Keegan, B. C.; Ogura, T.; Kim, S. H.; Ohta, T.; Baik, M.-H.; Ray, K.; Shearer, J.; Nam, W. Synthesis and reactivity of a mononuclear non-haem cobalt(IV)-oxo complex. *Nat. Commun.* **2017**, *8*, 14839.
(26) Cui, P.; Wang, Q.; McCollom, S. P.; Manor, B. C.; Carroll, P. J.; Tomson, N. C. Ring-Size-Modulated Reactivity of Putative Dicobalt-Bridging Nitrides: C-H Activation versus Phosphinimide Formation. *Angew. Chem., Int. Ed.* **2017**, *56* (50), 15979−15983.
(27) Maity, A. K.; Metta-Magana, A. J.; Fortier, S. Donor Properties of a New Class of Guanidinate Ligands Possessing Ketimine Backbones: A Comparative Study Using Iron. *Inorg. Chem.* **2015**, *54* (20), 10030−10041.
(28) Maity, A. K.; Murillo, J.; Metta-Magana, A. J.; Pinter, B.; Fortier, S. A Terminal Iron(IV) Nitride Supported by a Super Bulky Guanidinate Ligand and Examination of Its Electronic Structure and Reactivity. *J. Am. Chem. Soc.* **2017**, *139* (44), 15691−15700.
(29) Fortier, S.; Le Roy, J. J.; Chen, C. H.; Vieru, V.; Murugesu, M.; Chibotaru, L. F.; Mindiola, D. J.; Caulton, K. G. A Dinuclear Cobalt Complex Featuring Unprecedented Anodic and Cathodic Redox Switches for Single-Molecule Magnet Activity. *J. Am. Chem. Soc.* **2013**, *135* (39), 14670−14678.
(30) Fortier, S.; Moral, O. G. D.; Chen, C. H.; Pink, M.; Le Roy, J. J.; Murugesu, M.; Mindiola, D. J.; Caulton, K. G. Probing the redox non-innocence of dinuclear, three-coordinate Co(II) nindigo complexes: not simply beta-diketiminate variants. *Chem. Commun.* **2012**, *48* (90), 11082−11084.
(31) Chaudhuri, P.; Wagner, R.; Khanra, S.; Weyhermuller, T. Ferromagnetic vs. antiferromagnetic coupling in bis($\mu$(2)-1,1-azido)-dinickel(II) with syn- and anti-conformations of the end-on azide bridges. *Dalton Trans.* **2006**, *41*, 4962−4968.
(32) Chipman, J. A.; Berry, J. F. Extraordinarily Large Ferromagnetic Coupling (J ≥ 150 cm(−1)) by Electron Delocalization in a Heterometallic Mo(sic)Mo-Ni Chain Complex. *Chem. - Eur. J.* **2018**, *24* (7), 1494−1499.
(33) Wu, B. Y.; Yang, C. I.; Nakano, M.; Lee, G. H. Ferromagnetic interaction and slow magnetic relaxation in a Co-3 cluster-based three-dimensional framework. *Dalton Trans.* **2014**, *43* (1), 47−50.
(34) Cirera, J.; Jiang, Y.; Qin, L.; Zheng, Y. Z.; Li, G. H.; Wu, G.; Ruiz, E. Ferromagnetism in polynuclear systems based on non- linear [(Mn2MnIII)-Mn-II] building blocks. *Inorg. Chem. Front.* **2016**, *3* (10), 1272−1279.
(35) Mondal, M.; Chakraborty, M.; Drew, M. G. B.; Ghosh, A. Ni(II) Dimers of NNO Donor Tridentate Reduced Schiff Base Ligands as Alkali Metal Ion Capturing Agents: Syntheses, Crystal Structures and Magnetic Properties. *Magnetochemistry* **2018**, *4* (4), 51.
(36) Jones, C.; Schulten, C.; Rose, R. P.; Stasch, A.; Aldridge, S.; Woodul, W. D.; Murray, K. S.; Moubaraki, B.; Brynda, M.; La Macchia, G.; Gagliardi, L. Amidinato- and Guanidinato-Cobalt(I) Complexes: Characterization of Exceptionally Short Co-Co Interactions. *Angew. Chem., Int. Ed.* **2009**, *48* (40), 7406−7410.
(37) Tornieporth-Oetting, I. C.; Klapotke, T. M. Covalent Inorganic Azides. *Angew. Chem., Int. Ed. Engl.* **1995**, *34* (5), 511−520.
(38) Shin, J. H.; Bridgewater, B. M.; Churchill, D. G.; Baik, M.-H.; Friesner, R. A.; Parkin, G. An Experimental and Computational Analysis of the Formation of the Terminal Nitrido Complex ($\eta$3-Cp*)2Mo(N)(N3) by Elimination of N2 from Cp*2Mo(N3)2: The Barrier to Elimination Is Strongly Influenced by the exo versus endo Configuration of the Azide Ligand. *J. Am. Chem. Soc.* **2001**, *123* (41), 10111−10112.
(39) Costa, M.; Della Pergola, R.; Fumagalli, A.; Laschi, F.; Losi, S.; Macchi, P.; Sironi, A.; Zanello, P. Mixed Co-Rh nitrido-encapsulated carbonyl clusters. Synthesis, solid-state structure, and electrochemical/EPR characterization of the anions $[Co_{10}Rh(N)_2(CO)_{21}]^{3-}$, $[Co_{10}Rh_2(N)_2(CO)_{24}]^{2-}$, and $[Co_{11}Rh(N)_2(CO)^{24}]^{2-}$. *Inorg. Chem.* **2007**, *46* (2), 552−560.
(40) Hu, X. L.; Meyer, K. Terminal cobalt(III) imido complexes supported by tris(carbene) ligands: Imido insertion into the cobalt-carbene bond. *J. Am. Chem. Soc.* **2004**, *126* (50), 16322−16323.


https://dx.doi.org/10.1021/jacs.0c00291
J. Am. Chem. Soc. 2020, 142, 8233−8242

(41) Gloaguen, Y.; Rebreyend, C.; Lutz, M.; Kumar, P.; Huber, M.; van der Vlugt, J. I.; Schneider, S.; de Bruin, B. An Isolated Nitridyl Radical-Bridged {Rh(N.)Rh} Complex. *Angew. Chem., Int. Ed.* **2014**, *53* (26), 6814−6818.
(42) Sarkar, S.; Datta, A.; Mondal, A.; Chopra, D.; Ribas, J.; Rajak, K. K.; Sairam, S. M.; Pati, S. K. Competing Magnetic Interactions in a Dinuclear Ni(II) Complex: Antiferromagnetic O-H···O Moiety and Ferromagnetic N3- Ligand. *J. Phys. Chem. B* **2006**, *110* (1), 12−15.
(43) Gomez-Coca, S.; Ruiz, E. A density functional theory approach to the magnetic properties of a coupled single-molecule magnet (Mn-7)(2) complex - An entangled qubit pair candidate. *Can. J. Chem.* **2013**, *91* (9), 866−871.
(44) Zhao, J.; Li, D. S.; Wu, Y. P.; Yang, J. J.; Dong, W. W.; Zou, K. A rare pentanuclear Cu-II-based coordination framework exhibiting coexistence of antiferromagnetic and ferromagnetic couplings. *Inorg. Chem. Commun.* **2013**, *35*, 61−64.
(45) Maruyama, T.; Namekata, A.; Sakiyama, H.; Kikukawa, Y.; Hayashi, Y. Redox active mixed-valence hexamanganese double-cubane complexes supported by tetravanadates. *New J. Chem.* **2019**, *43* (45), 17703−17710.
(46) Duan, Y.; Clemente-Juan, J. M.; Gimenez-Saiz, C.; Coronado, E. Large Magnetic Polyoxometalates Containing the Cobalt Cubane '$[(Co^{III}Co_3^{III}(OH)_3(H_2O)_{6-m}(PW_9O_{34})]^{3-}$' (m = 3 or 5) as a Subunit. *Front. Chem.* **2018**, *6*, 231.
(47) Eckert, N. A.; Vaddadi, S.; Stoian, S.; Lachicotte, R. J.; Cundari, T. R.; Holland, P. L. Coordination-number dependence of reactivity in an imidoiron(III) complex. *Angew. Chem., Int. Ed.* **2006**, *45* (41), 6868−6871.
(48) Baek, Y.; Betley, T. A. Catalytic C-H Amination Mediated by Dipyrrin Cobalt Imidos. *J. Am. Chem. Soc.* **2019**, *141* (19), 7797−7806.
(49) Man, W. L.; Lam, W. W. Y.; Kwong, H. K.; Yiu, S. M.; Lau, T. C. Ligand-Accelerated Activation of Strong C-H Bonds of Alkanes by a (Salen)ruthenium(VI)-Nitrido Complex. *Angew. Chem., Int. Ed.* **2012**, *51* (36), 9101−9104.
(50) Marsh, R. E.; Thewalt, U. Structure of racemic. μ-amido-. μ-hydroxy-bis[bis(ethylenediamine)cobalt(III)] tetranitrate hydrate. *Inorg. Chem.* **1971**, *10* (8), 1789−1795.
(51) Dai, X. L.; Kapoor, P.; Warren, T. H. $[Me_2NN]Co(\eta(6)$-toluene): O = O, N = N, and O = N bond cleavage provides, beta-diketiminato cobalt μ-oxo and imido complexes. *J. Am. Chem. Soc.* **2004**, *126* (15), 4798−4799.
(52) Xue, X.-S.; Ji, P.; Zhou, B.; Cheng, J.-P. The Essential Role of Bond Energetics in C-H Activation/Functionalization. *Chem. Rev. (Washington, DC, U. S.)* **2017**, *117* (13), 8622−8648.
(53) Andris, E.; Navratil, R.; Jasik, J.; Terencio, T.; Srnec, M.; Costas, M.; Roithova, J. Chasing the Evasive Fe = O Stretch and the Spin State of the Iron(IV)-Oxo Complexes by Photodissociation Spectroscopy. *J. Am. Chem. Soc.* **2017**, *139* (7), 2757−2765.
(54) Andris, E.; Navratil, R.; Jasik, J.; Srnec, M.; Rodriguez, M.; Costas, M.; Roithova, J. M-O Bonding Beyond the Oxo Wall: Spectroscopy and Reactivity of Cobalt(III)-Oxyl and Cobalt(III)-Oxo Complexes. *Angew. Chem., Int. Ed.* **2019**, *58* (28), 9619−9624.
(55) Holscher, M.; Leitner, W. Catalytic NH3 Synthesis using N-2/H-2 at Molecular Transition Metal Complexes: Concepts for Lead Structure Determination using Computational Chemistry. *Chem. - Eur. J.* **2017**, *23* (50), 11992−12003.
(56) Brown, S. D.; Mehn, M. P.; Peters, J. C. Heterolytic H-2 activation mediated by low-coordinate L3Fe-(μ-N)-FeL3 complexes to generate Fe(μ-NH)(μ-H)Fe species. *J. Am. Chem. Soc.* **2005**, *127* (38), 13146−13147.
(57) Askevold, B.; Nieto, J. T.; Tussupbayev, S.; Diefenbach, M.; Herdtweck, E.; Holthausen, M. C.; Schneider, S. Ammonia formation by metal-ligand cooperative hydrogenolysis of a nitrido ligand. *Nat. Chem.* **2011**, *3* (7), 532−537.
(58) Schendzielorz, F. S.; Finger, M.; Volkmann, C.; Wurtele, C.; Schneider, S. A Terminal Osmium(IV) Nitride: Ammonia Formation and Ambiphilic Reactivity. *Angew. Chem., Int. Ed.* **2016**, *55* (38), 11417−11420.
(59) Falcone, M.; Poon, L. N.; Tirani, F. F.; Mazzanti, M. Reversible Dihydrogen Activation and Hydride Transfer by a Uranium Nitride Complex. *Angew. Chem., Int. Ed.* **2018**, *57* (14), 3697−3700.


https://dx.doi.org/10.1021/jacs.0c00291
*J. Am. Chem. Soc.* 2020, 142, 8233−8242